Opto-Electronic Advances

CN 51-1781/TN ISSN (Print) 2096-4579 ISSN (Online) 2097-3993

Ultrafast all-optical modulation of wide-bandwidth pulses enabled by silicon-metasurfaces

Kaloyan Georgiev, Khosro Zangeneh Kamali, Anton A. Trifonov, Giulia Crotti, Lyuben Petrov, Stefan Georgiev, Hristo Iliev, Lei Xu, Unai Arregui Leon, Mohsen Rahmani, Giuseppe Della Valle, Ivan Buchvarov* and Dragomir Neshev*

Citation: Georgiev K, Kamali KZ, Trifonov AA et al. Ultrafast all-optical modulation of wide-bandwidth pulses enabled by silicon-metasurfaces. *Opto-Electron Adv* **9**, 260007 (2026).

https://doi.org/10.29026/oea.2026.260007

Received: 7 January 2026; Accepted: 9 May 2026; Published online: 3 June 2026

Related articles

On-chip light control of semiconductor optoelectronic devices using integrated metasurfaces

Cheng-Long Zheng, Pei-Nan Ni, Yi-Yang Xie, et al

Opto-Electronic Advances 2025, **8**(1): 240159 doi: 10.29026/oea.2025.240159

Emerging landscape of photonic bound states in the continuum for next-generation metadevices

Thi Thu Ha Do, Ronghui Lin, Daniil A. Shilkin, et al

Opto-Electronic Advances 2026, **9**(3): 250224 doi: 10.29026/oea.2026.250224

Spin-dependent amplitude and phase modulation with multifold interferences via single-layer diatomic all-silicon metasurfaces

Hui Li, Chenhui Zhao, Jie Li, et al

Opto-Electronic Science 2025, **4**(3): 240025 doi: 10.29026/oes.2025.240025

Multi-dimensional photodetection: from material intrinsic properties and metasurface engineering to silicon photonic integration

Wenqi Liu, Zilan Tang, Qingzhao Hua, et al

Opto-Electronic Technology 2026, **2**(1): 260001 doi: 10.29026/oet.2026.260001

More related articles in Opto-Electronic Journals Group website

Opto-Electronic Journals Group

https://www.oejournal.org

OE_Journal

@OptoElectronAdv

OEA | Opto-Electronic Advances

Article

September 2026, Vol. 9, No. 9

Open Access

Ultrafast all-optical modulation of wide-bandwidth pulses enabled by silicon-metasurfaces

Kaloyan Georgiev[1,2†], Khosro Zangeneh Kamali[3,4†], Anton A. Trifonov[2], Giulia Crotti[5], Lyuben Petrov[1,2], Stefan Georgiev[1], Hristo Iliev[1], Lei Xu[6], Unai Arregui Leon[5], Mohsen Rahmani[6], Giuseppe Della Valle[5], Ivan Buchvarov[1,2,7*] and Dragomir Neshev[2,3*]

Abstract: Semiconductor metasurfaces have emerged as an effective platform for all-optical modulation thanks to their resonant light confinement and the enhancement of ultrafast optical effects like the Kerr effect and free-carrier generation. However, their narrow resonance features also restrict the available bandwidth for efficient modulation. Here, we demonstrate that a kink-like transmission spectral profile of a silicon metasurface could enable high-contrast modulation of wide-bandwidth pulses. We studied the all-optical ultrafast transmission modulation of the silicon metasurface induced by free-carrier excitation in a pump-probe configuration at different polarizations. We achieved ultrafast modulation of 28% (10%) with a speed of 25 ps and a bandwidth of up to 14 nm (49 nm) for *y*- and *x*-polarizations, respectively. Our results open up new opportunities for high-contrast, all-optical modulation of short pulses, with applications in optical communications and computing.

Keywords: ultrafast tuning; metasurfaces; pump-probe spectroscopy; nanophotonics

DOI: 10.29026/oea.2026.260007 | CSTR: 32247.14.oea.2026.260007

Citation: Georgiev K, Kamali KZ, Trifonov AA et al. Ultrafast all-optical modulation of wide-bandwidth pulses enabled by silicon-metasurfaces. *Opto-Electron Adv* **9**, 260007 (2026).

1 Introduction

Conventional methods for modulating the intensity of monochromatic light typically involve light-interferometric techniques. However, as the bandwidth of the light increases, the coherence length decreases, causing these interferometric techniques to become less effective due to limited operational bandwidth. Currently, the intensity of broadband propagating light is primarily controlled using electro-optic devices and other types of optical switches. Unfortunately, these options are often bulky and require complex driving systems. Optical metasurfaces have emerged as a promising alternative to traditional optical switches[1], offering size and operational efficiency advantages due to their compact design and resonant optical properties. Metasurfaces consist of arrays of subwavelength-sized optical resonators that have garnered significant interest in the optics and photonics community because of their unique scattering effects. As such, optical metasurfaces are excellent tools for spatial beam shaping and steering, providing subwavelength control over the transmitted amplitude and phase of light.

Furthermore, the sensitivity of the optical resonances to both the geometric and material parameters of the resonators or the surrounding medium allows for the possibility of actively modulating the transmitted and reflected light. Metasurface modulation has been achieved by numerous methods, including thermo-optic[2], electro-optic[3], or liquid crystals, to mention a few. All these approaches, however, have strengths and shortcomings[4,5].

Received: 7 January 2026

Accepted: 9 May 2026

Published online: 3 June 2026

[1]Department of Physics, Sofia University St. Kliment Ohridski, Sofia 1164, Bulgaria; [2]John Atanasoff Center for Bio and Nano Photonics (JAC BNP), Sofia 1164, Bulgaria; [3]ARC Centre of Excellence for Transformative Meta-Optical Systems (TMOS), Dept. of Electronic Materials Engineering, Research School of Physics, Australian National University, ACT 2601, Australia; [4]Department of Physics, Chalmers University of Technology, Gothenburg 412 96, Sweden; [5]Dipartimento di Fisica - Politecnico di Milano, Milano 20133, Italy; [6]Advanced Optics and Photonics Laboratory, Department of Engineering, School of Science and Technology, Nottingham Trent University, Nottingham NG11 8NS, United Kingdom; [7]Institute of Solid State Physics, Bulgarian Academy of Sciences, Tsarigradsko Chaussee 72, Sofia 1784, Bulgaria.

[†]These authors contributed equally to this work.

*Correspondence: I Buchvarov, E-mail: Ivan.Buchvarov@phys.uni-sofia.bg; D Neshev, E-mail: Dragomir.Neshev@anu.edu.au

The metasurface modulation speed depends on the characteristic time of the stimuli dynamics needed to modify the material, such as the time required to change the orientation of the liquid crystals[6–8]; the speed of charge accumulation (or depletion) in the optical media[9,10], the heat conduction speed[2,11,12], chemical reaction time[13] or mechanical actuators[14–16]. The ultrafast nature of optical nonlinearities in materials, such as photoexcitation and charge recombination dynamics, makes all-optical tuning one of the fastest modulation methods[17]. Such ultrafast nonlinear dynamics have been widely studied by pump-probe spectroscopy. The carrier lifetime and optical nonlinear processes of various thin films made from different materials, including epsilon-near-zero (ENZ) materials, have been extensively studied[18–24]. ENZ materials are popular for ultrafast tuning because of their large nonlinearity and the ability to change their refractive index significantly upon optical pumping[25,26]. However, their low refractive index presents a challenge for efficient light coupling, which limits their practical use.

Optical dielectric metasurfaces can effectively resolve these issues. Although high-index dielectric materials exhibit only a slight relative change in refractive index compared to ENZ media, their higher damage threshold and the resonant nonlinear enhancement in metasurfaces offer an alternative for improved light modulation. So far, ultrafast metasurface modulation has been explored for applications including the tuning of reflectance[27], nonreciprocity[28,29], negative refraction[30], frequency conversion[31–33] and beam shaping[34]. Out of the different material platforms, semiconductor metasurfaces with various geometries have been studied for all-optical modulation of light[35–39]. Metasurfaces made of direct bandgap semiconductors, such as III-V materials[35,40,41] and indirect bandgap materials, like silicon[36,42,43] have been the focus of research. The index modulation is generally stronger in crystalline semiconductors because of the larger density of electronic states at the band edges, as recently shown in the giant reflectivity modulation of nonlocal resonances in silicon metasurfaces[44]. We note that the modulation depth is best measured by the absolute modulation of transmission or reflection, as the relative change of transmission ($\Delta T/T$) is often not a true indicator of the modulation strength, especially near the resonance wavelength, where $T \to 0$.

In all previous work, however, strong optical modulation has been achieved only within a narrow spectral range, as it depends on shifting a single resonance. Notably, the modulation depth is greater for high-Q (high-quality) factor metasurface resonances. However, this comes at the cost of a reduced bandwidth. Here, we introduce and demonstrate an original concept for achieving large, ultrafast modulation of metasurface transmission of broadband signals. Our approach is based on the design of a kink-like metasurface transmission spectrum that blueshifts under the influence of a strong pump. Our metasurface is made of crystalline silicon on sapphire, which is modulated based on the optical injection of free carriers. Exploring these features enabled us to achieve a large transmission modulation over a bandwidth of 49 nm with an incident pump fluence of 460 μJ/cm^2 (absorbed 37 μJ/cm^2) at 520 nm. The free-carrier switching time is approximately 25 ps, and the measured bandwidth permits switching of sub-50 fs laser pulses.

The concept behind ultrafast all-optical modulation of wide-bandwidth pulses is illustrated in Fig. 1. In the conventional scenario, shown in Fig. 1(a), switching the transmittance from a minimum to a maximum requires a spectral shift of the resonance wavelength. To achieve this, a metasurface that supports narrowband optical resonances facilitates the switching process, as only a small spectral shift is required to maximize modulation. However, such narrow resonances limit the modulation bandwidth, as the continuous shift in resonance with power results in a subsequent drop in transmission. This issue can be alleviated if the transmission spectrum exhibits a kink-like profile. For a kink-like transmission profile, the same amount of spectral shift can support intensity modulation of a broader bandwidth signal (Fig. 1(b)). Additionally, further blueshift in such a kink-like system broadens the modulated spectrum. In practice, designing resonances in a metasurface to produce a kink-like transmission (similar to a low-pass filter) is challenging. A more realistic example of a metasurface with a steeper slope on the blue side of the resonance compared to the red side is shown in Fig. 1(c). A blueshift in such a metasurface causes significant modulation on the

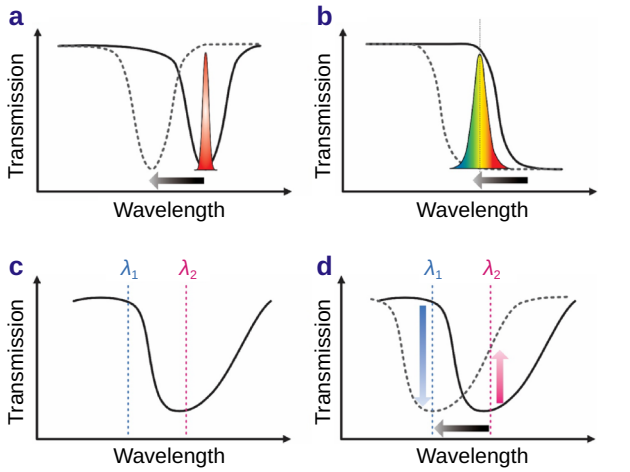

Fig. 1 | Concept of the ultrafast intensity modulation. (a) Transmission modulation by a metasurface featuring a high Q-factor resonance. Only narrowband spectral signals could be modulated. (b) Modulation by a kink-shaped transmission feature. The kink-like transmission supports the modulation of broadband spectral signals. (c) A realistic transmission spectrum of the resonance, featuring an asymmetrical kink-like resonance. The metasurface transmits light at λ_1, while it blocks light at λ_2. (d) When the kink resonance experiences a blue shift, the transmission intensity at λ_1 is significantly decreased, while the transmission intensity at λ_2 is not much affected.

blue side of the resonance (as seen in Fig. 1(d)), while the transmittance on the red side is only weakly affected. In the case of Fig. 1(d), the signal at λ_1 is modulated from on to off, while that at λ_2 is modulated from off to on. However, the opposite scenario could also be designed. These changes in the transmittance across different wavelengths result in the modulation of the total pulse intensity, in addition to pulse distortion[45] and frequency conversion arising from the time-varying nature of the metasurface modulation[46]. Pulse modulation is the main effect and the primary focus of this work. The impact of pulse distortion and frequency conversion depends on the specific shape of the incident pulse and is beyond the scope of the current study.

2 Results

2.1 Design and fabrication

The metasurface is designed to exhibit a kink-shaped response in the transmission spectra using a genetic algorithm (GA) approach, aiming to optimize a sharp, kink-like transmission feature at the desired wavelengths. Details on the GA calculations can be found in Section 1 of the Supplementary information. A 3D illustration of the optimized metasurface is shown in Fig. 2(a). A nominal metasurface consists of 100 nm thick crystalline silicon on a sapphire substrate, patterned to be a net square unit cell with a periodicity $p = 500$ nm, and an opening of $L_1 = 320$ nm and $W_1 = 250$ nm in the x and y axes, respectively. A particle with a width and length of $L_2 = 100$ nm and $W_2 = 120$ nm (in the x and y directions) is placed in the center of the net. Due to the asymmetry, the metasurface optical response depends on the incident polarization.

The simulated optimal design was fabricated using a standard electron-beam lithography (EBL) technique. First, a commercial crystalline silicon film (600 nm) on sapphire is etched down to a thickness of 100 nm using Inductively Coupled Plasma (ICP). Then, a diluted ZEP520A resist in anisole, with a volume ratio of 1:1, is spun onto the substrate. After exposing the pattern by EBL, the resist is developed, and the patterned resist is used as a dry etch mask. Subsequently, the silicon film is etched by a second step of ICP. The remaining resist mask is then removed by mild oxygen plasma treatment. Scanning Electron Microscope (SEM) images of the fabricated sample are shown in Fig. 2(b, c). Several metasurfaces of a size of 100 × 100 μm and different EBL exposures were fabricated.

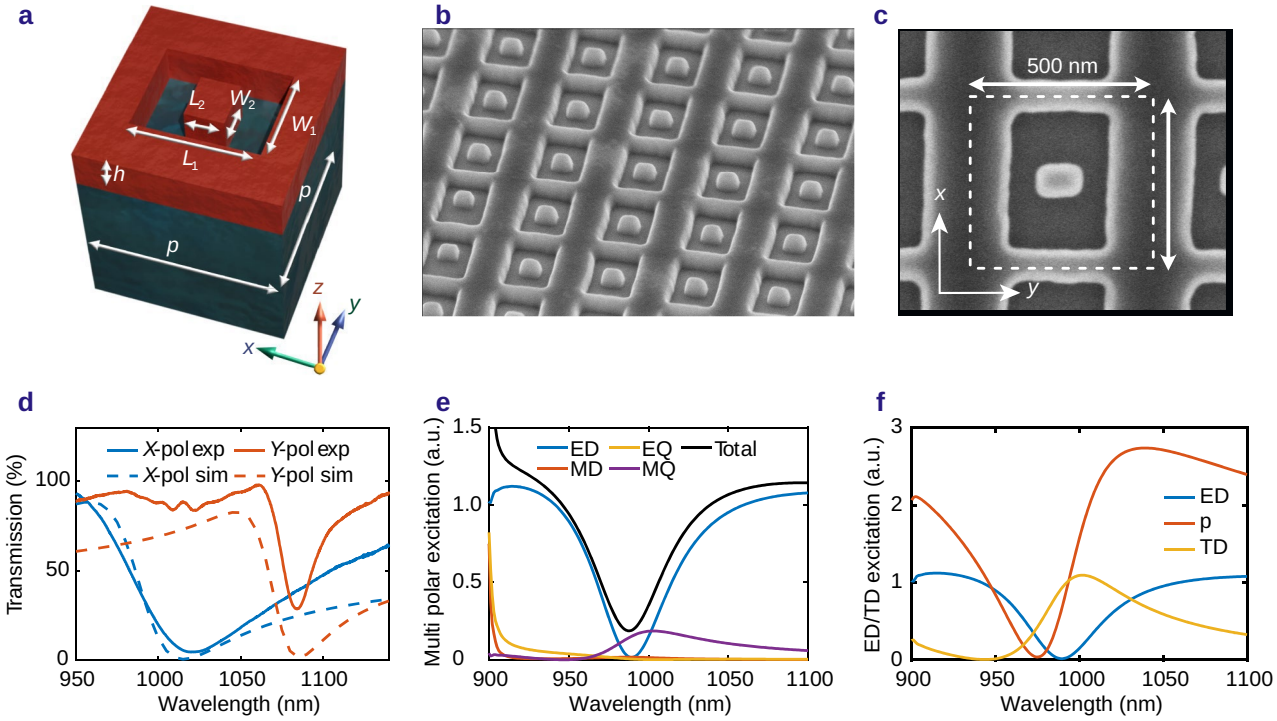

Fig. 2 | Design and fabrication of the metasurface. (a) Schematic diagram of the metasurface unit cell. The dimensions of the silicon structure are h = 100 nm, p = 500 nm, L_1 = 320 nm, W_1 = 250 nm, L_2 = 100 nm, and W_2 = 120 nm. (b) Top view and (c) angled view SEM image of the fabricated sample. (d) Measured (solid lines) and simulated (dashed lines) transmission spectra of the metasurface under x-polarized (blue) and y-polarized (orange) excitation at normal incidence. (e) Spherical multimode expansion and (f) Cartesian moment analysis of the metasurface, while excited with x-polarized light. In panels (d–f), the geometric parameters have been fitted to best match the experimental transmission spectra within the allowed fabrication tolerances. The updated parameters are: L_1^{fit} = 326 nm, W_1^{fit} = 228 nm, L_2^{fit} = 112 nm, and W_2^{fit} = 130 nm.

Figure 2(d) shows the simulated and experimentally measured metasurface transmission spectra under *x*- and *y*-polarization illumination. For the simulations, we employed fitted values for the geometrical parameters within the fabrication tolerances (see the figure caption). The measured spectra are in good agreement with the simulated resonant transmission features, particularly for *x*-polarization. The resonance in the *y*-polarization shows a slightly reduced contrast and steeper slope in the red wing with respect to the design. This slight deviation between the simulated and experimental results is due to the fabrication error, possible surface roughness, and discrepancies in the refractive index values of the film and the substrate. The kink-like transmission spectral response is achieved by engineering the optical modes excited in the metasurface, based on the mechanism of the symmetry-protected bound-state-in-the-continuum (BIC)[47]. The evolution of the Q-factor for the BIC mode and the formation of a kink-like Fano spectral shape in the optical response transmission spectrum are illustrated in Section 1 of the Supplementary information. In particular, the introduced structural asymmetry through the central cuboid breaks the in-plane symmetry, enabling independent control of the radiative leakage channels for the supported BIC modes along the *x*- and *y*-directions, respectively. Figure 2(e) shows the spherical multipole decomposition of the metasurface excited under *x*-polarized illumination by taking into account the first two orders of electric and magnetic multipoles: electric dipole (ED), magnetic dipole (MD), electric quadrupole (EQ), and magnetic quadrupole (MQ). As seen, the optical response is primarily dominated by the excitation of an *x*-oriented ED. To further understand the contributions of multipoles to the far-field response, we also performed the Cartesian multipole analysis, focusing on the ED and toroidal dipole (TD) components (see Fig. 2(f)). Our metasurface supports a symmetry-protected bound-state-in-the-continuum TD mode, serving as the nonradiative channel, and an ED serving as the leaky channel, which can be excited externally by a normally incident plane wave. By exciting the ED and through the coupling between the 'dark' TD mode and the 'bright' p_x-ED mode, a Fano resonance is formed to give the kink-like transmission spectral response (see Fig. 2(e)). By controlling the geometric parameter of the central nano cuboid, the radiation of the Fano resonance can be well controlled. Similar results are also obtained for the *y*-polarized input excitation and are shown in Fig. S6 of the Supplementary information. The multipolar components, however, are spectrally shifted to longer wavelengths.

2.2 Time-resolved pump-probe spectroscopy

Next, we tested the temporal dynamics of the all-optical modulation of the fabricated metasurface using time-resolved pump-probe spectroscopy. Figure 3(a) illustrates the pump-probe spectroscopy setup for measuring the dynamic metasurface response. We use a *y*-polarized pump beam at 520 nm, which has energy above the bandgap of the crystalline silicon, and where the metasurfaces exhibit no resonant features due to absorption. The pump is derived from a pulsed laser with pulses of 130 fs full-width at half maximum (FWHM) duration and a repetition rate of 1.4 kHz. The pump pulses have an energy of 39±5 nJ. The pump beam is mildly focused onto the metasurface to a beam diameter of 104±10 μm ($1/e^2$ level), resulting in an incident pump fluence of 460 μJ/cm^2. This fluence is chosen to be lower than the damage threshold of the metasurface. The latter was estimated to be around 1 mJ/cm^2 based on two accidental instances of sample damage. The incident pump power absorbed by the sample results in the photoexcitation of free carriers. The metasurface is subsequently illuminated at normal incidence by a broadband probe beam derived from supercontinuum generation, obtained by pumping a 6-mm-thick YAG crystal with 1250 nm femtosecond laser pulses. The probe beam is focused to a spot size of 70±7 μm (diameter at $1/e^2$ level). A delay path controls the time difference between the pump and the probe pulses on the sample.

Figure 3(b, c) display the transmission spectra of the metasurface at various delay times for *x*- and *y*-polarized probes, respectively. The metasurface undergoes a sudden blueshift in less than 0.5 ps. This shift is caused by the photoexcitation of free-carriers in crystalline silicon, which reduces the silicon's refractive index as the free-carrier density increases. Upon recombination of the induced charge carriers with time, the resonance returns to its initial state. The absolute (ΔT) and the relative transmission spectra ($\Delta T/T$) of the metasurface for both probe polarizations are shown in Fig. 4. Under *x*-polarized illumination, the spectrum displays a kink-like transmission response around 990 nm, which, after an initial blueshift, goes back to the steady state with the carrier relaxation. This allows the observation of larger absolute modulation at the short-wavelength range of the transmission dip (Fig. 4(a)). Comparing Fig. 4(a, b), one can notice that the highest relative transmission modulation ($\Delta T/T$) occurs near the resonant wavelength, where the static transmission is low, due to the division by a small value ($T \sim 0$). In practice, we observe a band of positive relative modulation at the longer wavelength range near the resonance and a negative modulation band at the shorter wavelength range near the resonance, both showing relative modulation of over 20%. Similar transient dynamics is also seen for the *y*-polarized probe, as shown in Fig. 4(d, e). The difference is the narrower bandwidth around 1080 nm and the larger absolute modulation of up to 28%.

The absolute dynamic modulation allows us to estimate the modulation bandwidth. The spectral bandwidth is estimated as the spectral range over which the absolute modulation $|\Delta T|$ exceeds 50% of its maximum. Notably, the metasurface design supports two modulation bands, one with stronger but negative ΔT at shorter wavelengths, which

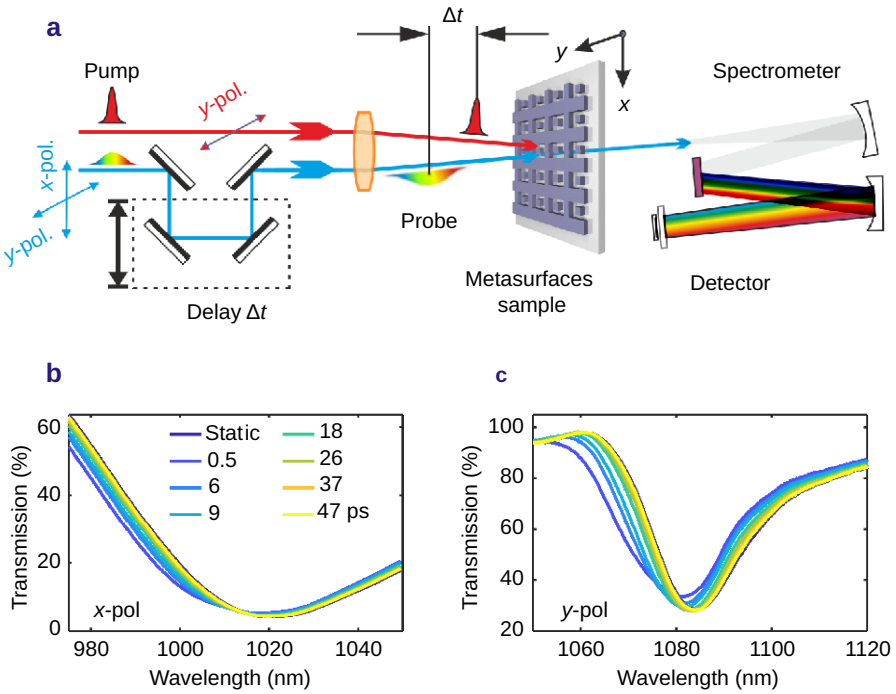

Fig. 3 | Pump-probe spectroscopy. (a) A schematic diagram of the pump-probe spectroscopy setup. (b, c) Transmission spectra of the metasurfaces for different delay times in picoseconds under *x*- and *y*-polarizations of the probe signal, respectively. The corresponding time delays are color-coded and given in the legend.

corresponds to a "switch-off" dynamic condition. The other band, at longer wavelengths, has positive ΔT, which corresponds to "switch-on" dynamic condition. The estimated bandwidths of the stronger modulation bands (see also SI, Fig. S7) are 49 nm and 14 nm under *x*- and *y*-polarized illumination, respectively. These bandwidth results illustrate the wide-bandwidth switching regime enabled by the kink-like spectral profile of our metasurfaces. In particular, the larger bandwidth of 49 nm (obtained with an *x*-polarized probe) is a direct consequence of the steady-state resonance shape, which more closely resembles the ideal asymmetric "kink" compared to the feature seen in *y*-polarization (see Fig. 2(d)). Note that this comparison quantitatively reflects our design concept, as illustrated in Fig. 1.

Figure 4(c, f) display the experimental transient relative transmission at various delay times for the wavelengths of peak modulation and *x*- and *y*-polarization, respectively. Photoexcitation and free carrier generation occur within the first 250 fs (see insets), as the optical field in the resonators is continually absorbed by the silicon. Since the resonators lack a resonance at the pump wavelength of 520 nm, the pump field is not confined within the structure. As a result, the pump lifetime inside the metasurface is similar to the pulse duration and matches the response of the plane silicon film. By measuring the reflection and transmission of the homogeneous thin film, we can experimentally estimate the pump absorption to be about 8%, corresponding to an absorbed pump fluence of $F_{\mathrm{abs}}^{\mathrm{exp}} = 37$ μJ/cm². We note that estimating the total absorption of the metasurface is particularly challenging due to strong diffraction within the substrate. When the modulation peak intensity reaches its peak value, the next modulation stage occurs in the absence of a pump field and the presence of the generated free carriers in the crystalline silicon. Based on the free carriers' lifetime in the material, photoexcited electron-hole pairs recombine and release their energy as heat. The free carriers take approximately 25 ps to halve their concentration and less than 100 ps to recombine completely. At this timescale, the silicon refractive index reverts to its original value, as the free carrier concentration declines over time. This results in a reduction in the amplitude of transient transmission intensity. In the absence of the free carriers and the optical field ($>$ 100 ps), we see a slight change in the direction of the transient transmission intensity, indicating a redshift in the metasurface resonance wavelength. This is attributed to the heat generated during carrier recombination, which subsequently increases the refractive index of the silicon due to the thermo-optic effect. Since the thermo-optic coefficient of the silicon is positive, we correspondingly observe a redshift in the resonance wavelength. The thermo-optical effect disappears at times longer than ~1 ns.

2.3 Simulations of the modulation dynamics

Next, we develop a quantitative model to describe the transient transmission modulation dynamics of our experiments.

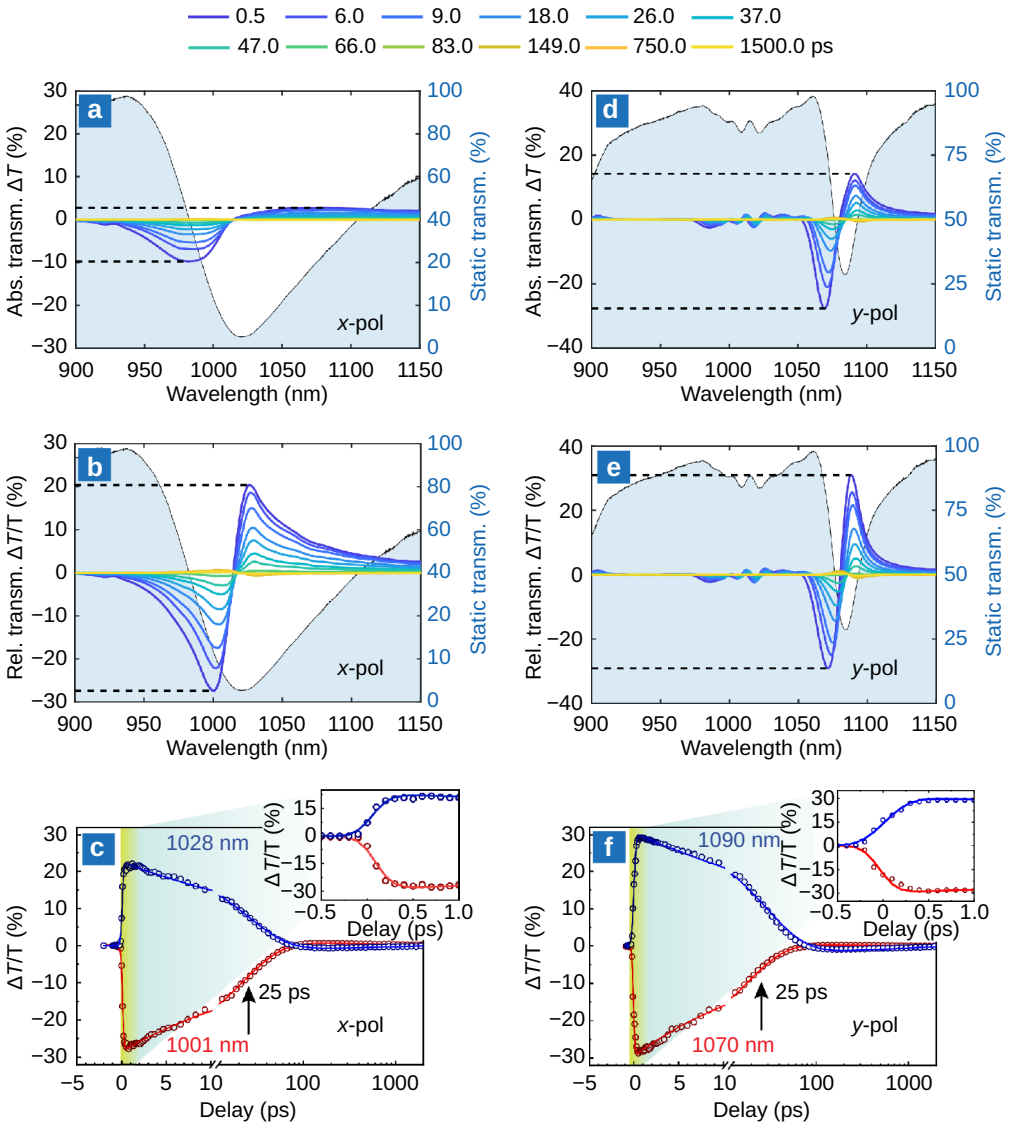

Fig. 4 | Metasurface modulation dynamics. (a) and (b) are the absolute and relative transmission modulation when illuminated by an *x*-polarized light. (c) The relative transmission modulation of the metasurface excited by *x*-polarized light at wavelengths of 1001 nm and 1028 nm. Panels (d) and (e) show the absolute and relative transmission modulation when illuminated by a *y*-polarized light. (f) Relative transmission modulation of the metasurface excited by *y*-polarized light at wavelengths of 1070 nm and 1090 nm. The inset image in (c) and (f) shows the temporal magnified snapshot of the intensity modulation of the corresponding graphs for delay times <1 ps.

The model assumptions are summarized below (see also ref.[43]). Upon illumination by a pump pulse of given fluence, a population of electron-hole pairs is photogenerated in the crystalline silicon structure. In view of the pump photon energy, which is well above the silicon bandgap, we consider only linear (single photon) processes as the dominant contribution to absorption. Then, the free-carrier population undergoes relaxation processes. We take into account trap-assisted recombination, bimolecular recombination, and the three-body Auger effect. This last contribution, which is dominant in bulk configurations, is instead comparatively small in our system, i.e., a nanostructured material with a large surface-to-volume ratio. The dominant effect indeed comes from the trap-assisted, non-radiative recombination from surface defects[48]. Each recombination is accompanied by phonon emission, which gradually increases the lattice temperature. The evolution of the two dynamical variables $N(t)$, representing carrier density, and $\Theta_L(t)$, representing the lattice temperature, is modelled by a rate-equation system. In turn, these internal degrees of freedom are responsible for the transient modulation of the system permittivity, $\Delta\varepsilon(t)$. Specifically, the presence of the electron-hole plasma, described by the density $N(t)$, entails a modification of intraband transitions with a Drude-like contribution to $\Delta\varepsilon$, conversely, the lattice temperature increase causes a thermo-optical effect. Having estimated

the total $\Delta\varepsilon$ as a function of time and probe wavelength through semiclassical formulas, it is possible to understand how the optical response is modulated in time via a simple perturbative approach. By exploiting full-wave electromagnetic simulations to obtain the transmission T under unperturbed conditions and upon small perturbations of permittivity (real and imaginary part, respectively), it is possible to extract the coefficients χ, ψ of the linearized function $T(\varepsilon+\Delta\varepsilon) = T\left(\varepsilon+\Delta\varepsilon^{'}+\mathrm{i}\Delta\varepsilon^{''}\right)$, and therefore compute it as a function of probe wavelength and pump-probe time delay: $T(\lambda_{\mathrm{probe}}, t) = T(\varepsilon) + \chi\Delta\varepsilon^{'}(\lambda_{\mathrm{probe}}, t) + \psi\Delta\varepsilon''(\lambda_{\mathrm{probe}}, t)$. A more detailed description is provided in the Supplementary information Section 3.

The plots in Fig. 5(a, b) show the experimental and simulated transient relative transmission spectra of the metasurface with *y*-polarized probe illumination at different delay times. In our finite element method simulations, we used an absorbed pump fluence of 45 μJ/cm^2, which is of the same order as that observed in our experiments. Notably, the transmission modulation reaches its peak shortly after the sample is illuminated with the pump. Then, as the charges recombine in time, the signal gradually returns to its static value. A direct comparison of the transient transmission at five different wavelengths is shown in Fig. 5(c). The agreement between the experimental and modeled data maps demonstrates the model's validity in predicting the metasurface's transient behavior, despite the slightly different excitation flux levels. The slight difference in the experimental and simulated modulation amplitudes can be attributed to finite-size effects, unavoidable inhomogeneities or defects, and deviations from exact periodicity in the fabricated structure. We note that if we choose slightly red-shifted nominal wavelengths of up to 5 nm (less than 10% of the resonance width), we observe a significantly improved agreement between theory and experiment. Similar dependencies for experimental and simulated data, using *x*-polarized illumination, are shown in Section 4 of the Supplementary information.

The numerical simulations further provide access to the transient absorption of the metasurface, which is difficult to obtain in our experiments. The calculated absolute absorption for *y*-polarized illumination is depicted in Fig. 5(d). The results show that the free carriers induce significant absorption in the metasurface for over 30 ps. The peak absorption is just over 4% and happens at the peak free-carrier concentration. This extra absorption has to be accounted for in possible future applications of the observed ultrafast optical modulation, including time-variant metasurfaces for frequency conversion or Floquet physics with periodic time drives.

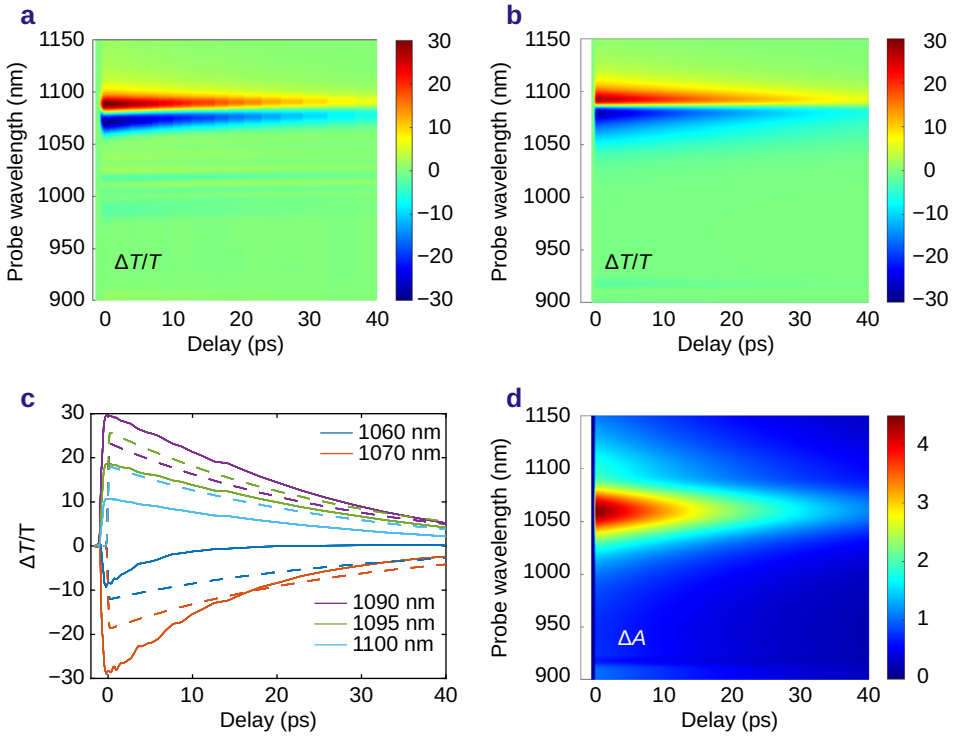

Fig. 5 | Numerical simulations and comparison to the experiments. (a, b) Experimental and calculated data, respectively, representing the relative transmission intensity modulation under *y*-polarization illumination. (c) Comparison of the relative transmission modulation between experimental (solid line) data and the model (dashed line) under *y*-polarized probe illumination. (d) The calculated absolute absorption spectra in percent at different delay times.

3 Conclusions

In summary, we proposed and demonstrated a novel concept for the ultrafast modulation of wide-bandwidth signals using silicon metasurfaces that exhibit kink-like transmission spectral features. The kink-like metasurface transmission is designed by genetic algorithm optimization in the near-infrared spectral region. It achieves a sharp transmission front by the interference of a dark-state narrowband toroidal dipole resonance with a bright electric dipole broadband response. This asymmetric transmission profile, characterized by a sharp transmission kink followed by a broad transmission dip at longer wavelengths, is successfully utilized to modulate broadband optical signals. For this purpose, the metasurface is pumped by femtosecond green laser pulses (520 nm) with a repetition rate of 1.4 kHz and an input pulse fluence of 460 μJ/cm^2. A broadband probe is used to test the ultrafast modulation of the metasurface transmission. We have demonstrated that the steep transmission change in the proposed metasurface results in 28% absolute transmission modulation with a bandwidth of 14 nm for *y*-polarized signals and 10% modulation with a bandwidth of 49 nm for *x*-polarized signals. Our results compare favorably with other all-optical modulation experiments[39,49]. For a more comprehensive comparison, see Table S1 in Section 5 of the Supplementary information, which lists essential parameters for evaluating performance. Many studies do not provide enough data or are conducted under varying experimental conditions, complicating direct comparisons. Nevertheless, our results demonstrate broad-spectrum band modulation at moderate absorbed fluences. An important metric for comparison is the modulation bandwidth per absorbed fluence, which normalizes the bandwidth relative to the applied power. Based on existing data, our modulation performance surpasses that of similar studies using conventional resonant designs. Consequently, we conclude that the kink-shaped spectral profile provides the broadest bandwidth modulation for a given absorbed fluence.

Our results, therefore, demonstrate the potential of optical metasurfaces to modulate wide-bandwidth optical signals with high contrast and ultrafast speed. This potential opens new opportunities for efficient adiabatic frequency conversion and novel Floquet physics with periodically modulated materials[50]. On the practical side, the ultrafast modulation of the optical properties of the transmitted pulses could find important applications for spatiotemporal pulse shaping[51] and ultra-fast Light Detection and Ranging (LiDAR)[52]. Notably, the moderate modulation depth of 10%–30% could be particularly useful in applications such as optical communications, laser mode locking, and, most recently, photonic neuromorphic reservoir computing, where 30% contrast is enough for analogue weighting or multiplication. In all such applications, the modulation depth achieved in our experiments is practical and already commonly used.

References

1. Mikheeva E, Kyrou C, Bentata F et al. Space and time modulations of light with metasurfaces: recent progress and future prospects. *ACS Photonics* **9**, 1458–1482 (2022).
2. Zangeneh Kamali K, Xu L, Gagrani N et al. Electrically programmable solid-state metasurfaces via flash localised heating. *Light Sci Appl* **12**, 40 (2023).
3. Benea-Chelmus I C, Meretska M L, Elder D L et al. Electro-optic spatial light modulator from an engineered organic layer. *Nat Commun* **12**, 5928 (2021).
4. Shaltout A M, Shalaev V M, Brongersma M L. Spatiotemporal light control with active metasurfaces. *Science* **364**, eaat3100 (2019).
5. Neshev D N, Miroshnichenko A E. Enabling smart vision with metasurfaces. *Nat Photon* **17**, 26–35 (2023).
6. Fréedericksz V, Zolina V. Forces causing the orientation of an anisotropic liquid. *Trans Faraday Soc* **29**, 919–930 (1933).
7. Frisken B J, Palffy-Muhoray P. Freedericksz transitions in nematic liquid crystals: the effects of an in-plane electric field. *Phys Rev A* **40**, 6099–6102 (1989).
8. Thalhammer G, Bowman R W, Love G D et al. Speeding up liquid crystal SLMs using overdrive with phase change reduction. *Opt Express* **21**, 1779–1797 (2013).
9. Yao Y, Kats M A, Genevet P et al. Broad electrical tuning of graphene-loaded plasmonic antennas. *Nano Lett* **13**, 1257–1264 (2013).
10. Kafaie Shirmanesh G, Sokhoyan R, Pala R A et al. Dual-gated active metasurface at 1550 nm with wide (>300°) phase tunability. *Nano Lett* **18**, 2957–2963 (2018).
11. Zhang Y F, Fowler C, Liang J H et al. Electrically reconfigurable non-volatile metasurface using low-loss optical phase-change material. *Nat Nanotechnol* **16**, 661–666 (2021).
12. Abdollahramezani S, Hemmatyar O, Taghinejad M et al. Electrically driven reprogrammable phase-change metasurface reaching 80% efficiency. *Nat Commun* **13**, 1696 (2022).
13. Li J X, Kamin S, Zheng GX et al. Addressable metasurfaces for dynamic holography and optical information encryption. *Sci Adv* **4**, eaar6768 (2018).
14. Ee H S, Agarwal R. Tunable metasurface and flat optical zoom lens on a stretchable substrate. *Nano Lett* **16**, 2818–2823 (2016).
15. Afridi A, Gieseler J, Meyer N et al. Ultrathin tunable optomechanical metalens. *Nano Lett* **23**, 2496–2501 (2023).
16. Thrane P C V, Meng C, Ding F et al. MEMS tunable metasurfaces based on gap plasmon or Fabry–Pérot resonances. *Nano Lett* **22**, 6951–6957 (2022).
17. Shcherbakov M, Liu S, Brener I et al. Nonlinear and ultrafast effects. In Brener I, Liu S, Staude I et al. *Dielectric Metamaterials: Fundamentals, Designs, and Applications* (Woodhead Publishing, Duxford, 2020).
18. Kinsey N, Devault C, Kim J et al. Epsilon-near-zero Al-doped ZnO for ultrafast switching at telecom wavelengths. *Optica* **2**, 616–622 (2015).
19. Sabbah A J, Riffe D M. Femtosecond pump-probe reflectivity study of silicon carrier dynamics. *Physical Review B* **66**, 165217 (2002).
20. Clerici M, Kinsey N, DeVault C et al. Controlling hybrid nonlinearities in transparent conducting oxides via two-colour excitation. *Nat Commun* **8**, 15829 (2017).
21. Harmon E S, Melloch M R, Woodall J M et al. Carrier lifetime versus anneal in low temperature growth GaAs. *Appl Phys Lett* **63**, 2248–2250 (1993).
22. Saha S, Dutta A, DeVault C et al. Extraordinarily large permittivity modulation in zinc oxide for dynamic nanophotonics. *Mater Today* **43**, 27–36 (2021).
23. Tirole R, Vezzoli S, Galiffi E et al. Double-slit time diffraction at optical frequencies. *Nat Phys* **19**, 999–1002 (2023).
24. Grinblat G, Nielsen M P, Dichtl P et al. Ultrafast sub–30-fs all-optical switching based on gallium phosphide. *Sci Adv* **5**, eaaw3262 (2019).
25. Kim K H. Unity-order nonlinear optical index change in epsilon-near-zero composite materials of gain media and metal nanoparticles. *Annalen der Physik* **530**, 1700259 (2018).

26. Alam M Z, De Leon I, Boyd R W. Large optical nonlinearity of indium tin oxide in its epsilon-near-zero region. *Science* **352**, 795–797 (2016).
27. Makarov S, Kudryashov S, Mukhin I et al. Tuning of magnetic optical response in a dielectric nanoparticle by ultrafast photoexcitation of dense electron–hole plasma. *Nano Lett* **15**, 6187–6192 (2015).
28. Barati Sedeh H, Mohammadi Dinani H, Mosallaei H. Optical nonreciprocity via transmissive time-modulated metasurfaces. *Nanophotonics* **11**, 4135–4148 (2022).
29. Shaltout A, Kildishev A, Shalaev V. Time-varying metasurfaces and Lorentz non-reciprocity. *Opt Mater Express* **5**, 2459–2467 (2015).
30. Bruno V, DeVault C, Vezzoli S et al. Negative refraction in time-varying strongly coupled plasmonic-antenna-epsilon-near-zero systems. *Phys Rev Lett* **124**, 043902 (2020).
31. Shcherbakov M R, Werner K, Fan Z Y et al. Photon acceleration and tunable broadband harmonics generation in nonlinear time-dependent metasurfaces. *Nat Commun* **10**, 1345 (2019).
32. Lee K, Son J, Park J et al. Linear frequency conversion via sudden merging of meta-atoms in time-variant metasurfaces. *Nat Photon* **12**, 765–773 (2018).
33. Karl N, Vabishchevich P P, Shcherbakov M R et al. Frequency conversion in a time-variant dielectric metasurface. *Nano Lett* **20**, 7052–7058 (2020).
34. Karimi M, Alam Z, Upham J et al. Time-varying gradient metasurface with applications in all-optical beam steering. *Nanophotonics* **12**, 1733–1740 (2023).
35. Shcherbakov M R, Liu S, Zubyuk V V et al. Ultrafast all-optical tuning of direct-gap semiconductor metasurfaces. *Nat Commun* **8**, 17 (2017).
36. Shcherbakov M R, Vabishchevich P P, Shorokhov A S et al. Ultrafast all-optical switching with magnetic resonances in nonlinear dielectric nanostructures. *Nano Lett* **15**, 6985–6990 (2015).
37. Grinblat G, Zhang H Z, Nielsen M P et al. Efficient ultrafast all-optical modulation in a nonlinear crystalline gallium phosphide nanodisk at the anapole excitation. *Sci Adv* **6**, eabb3123 (2020).
38. Lemasters R, Shcherbakov M R, Yang G C et al. Deep optical switching on subpicosecond timescales in an amorphous Ge metamaterial. *Adv Opt Mater* **9**, 2100240 (2021).
39. Crotti G, Akturk M, Schirato A et al. Giant ultrafast dichroism and birefringence with active nonlocal metasurfaces. *Light Sci Appl* **13**, 204 (2024).
40. Vabishchevich P P, Vaskin A, Karl N et al. Ultrafast all-optical diffraction switching using semiconductor metasurfaces. *Appl Phys Lett* **118**, 211105 (2021).
41. Shilkin D A, Ha S T, Paniagua-Domínguez R et al. Ultrafast modulation of a nonlocal semiconductor metasurface under spatially selective optical pumping. *Nano Lett* **24**, 14229–14235 (2024).
42. Yang Y M, Wang W Y, Boulesbaa A et al. Nonlinear fano-resonant dielectric metasurfaces. *Nano Lett* **15**, 7388–7393 (2015).
43. Della Valle G, Hopkins B, Ganzer L et al. Nonlinear anisotropic dielectric metasurfaces for ultrafast nanophotonics. *ACS Photonics* **4**, 2129–2136 (2017).
44. Tognazzi A, Franceschini P, Sergaeva O, et al. Giant photoinduced reflectivity modulation of nonlocal resonances in silicon metasurfaces. *Adv Photon* **5**, 066006 (2023).
45. Basiri A, Rafique Z E, Bai J et al. Ultrafast low-pump fluence all-optical modulation based on graphene-metal hybrid metasurfaces. *Light Sci Appl* **11**, 102 (2022).
46. Yang Z W, Liu M K, Smirnova D et al. Ultrafast Q-boosting in semiconductor metasurfaces. *Nanophotonics* **13**, 2173–2182 (2024).
47. Hsu C W, Zhen B, Stone A D et al. Bound states in the continuum. *Nat Rev Mater* **1**, 16048 (2016).
48. Dan Y P, Seo K, Takei K et al. Dramatic reduction of surface recombination by in situ surface passivation of silicon nanowires. *Nano Lett* **11**, 2527–2532 (2011).
49. Karl N, Vabishchevich P P, Liu S et al. All-optical tuning of symmetry protected quasi bound states in the continuum. *Appl Phys Lett* **115**, 141103 (2019).
50. Galiffi E, Tirole R, Yin S X, et al. Photonics of time-varying media. *Adv Photon* **4**, 014002 (2022).
51. Zhang F, Bao H L, Pu M B et al. Dispersion-engineered spin photonics based on folded-path metasurfaces. *Light Sci Appl* **14**, 198 (2025).
52. Gong S J, Guo Y H, Li X Y et al. Spectral-acoustic-coordinated astigmatic metalens for wide field-of-view and high spatiotemporal resolution 3D imaging. *Light Sci Appl* **15**, 85 (2026).

Acknowledgements

This work was supported by the Australian Research Council under the Centre of Excellence for Transformative Meta-Optical Systems (TMOS) (CE200100010). The sample fabrication was supported by the Australian National Fabrication Facility (ACT node). This publication is part of the METAFAST project that received funding from the European Union Horizon 2020 Research and Innovation program under Grant Agreement No. 899673. GDV and UAL acknowledge the support from the HOTMETA project under the PRIN 2022 MUR programme funded by the European Union - Next Generation EU - "PNRR —M4C2, investimento 1.1 - "Fondo PRIN 2022" —HOT-carrier METasurfaces for Advanced photonics (HOTMETA), contract no. 2022LENW33 —CUP: D53D2300229 0006". IB, LP, SG, and HI acknowledge support by the Ministry of Education and Science of Bulgaria (HEPHAESTUS grant) of the Bulgarian National Roadmap for Research Infrastructure. I.B. and A.T. acknowledge financial support by the European Union-NextGenerationEU, through the National Recovery and Resilience Plan of the Republic of Bulgaria, SUMMIT BG-RRP-2.004-0008-C0. MR and LX acknowledge support from the UK Research and Innovation Future Leaders Fellowship (MR/Z000270/1).MR appreciates the support from ERC Consolidator Grant (UPIRI, 101170298). Views and opinions expressed are, however, those of the authors only and do not necessarily reflect those of the European Research Council.

Competing interests

The authors declare no competing financial interests.

Supplementary information

Supplementary information for this paper is available at
https://doi.org/10.29026/oea.2026.260007

Open Access This article is licensed under a Creative Commons Attribution 4.0 International License, which permits use, sharing, adaptation, distribution and reproduction in any medium or format, as long as you give appropriate credit to the original author(s) and the source, provide a link to the Creative Commons license, and indicate if changes were made. To view a copy of this license, visit
http://creativecommons.org/licenses/by/4.0/
©The Author(s) 2026.
Published by Editorial Office of *Opto-Electronic Advance*, Institute of Optics and Electronics, Chinese Academy of Sciences.

Opto-Electronic Journals Group
www.oejournal.org
Scan for Article PDF